On the inclusion of structural loading and damping in piezoelectric shunt tuning

Toftekær, Johan Frederik; Høgsberg, Jan

Published in:
Journal of Sound and Vibration

Link to article, DOI:
10.1016/j.jsv.2021.115960

Publication date:
2021

Document Version
Peer reviewed version

On the inclusion of structural loading and damping in piezoelectric shunt tuning

Johan Frederik Toftekær[a,*], Jan Høgsberg[a]

[a]*Department of Mechanical Engineering,*
Technical University of Denmark,
DK-2800 Kongens Lyngby, Denmark
Nils Koppels Allé, Building 404

Abstract

Expressions for piezoelectric inductive-resistive shunt tuning to a targeted structure mode are obtained by explicit frequency response functions, derived from a combined short- and open-circuit modal representation that accounts for inherent structural damping. The influence of external loading is further included by accounting for the short-circuit dynamic and quasi-static contributions from modes below and above the target mode, respectively. This augmented representation provides accurate frequency response for displacement and electric charge and voltage, and thus be generally used to derive desired shunt tuning strategies. Presently, explicit tuning expressions are based on a flat plateau condition in the voltage amplitude for a parallel inductive-resistive shunt or the charge amplitude for the corresponding series shunt. The tuning robustness with respect to changes in structural damping and external load distributions is verified by a numerical benchmark problem, which further shows that the explicit frequency response functions precisely predict the full structural and electric response around the targeted structure mode. This result can help bypass the need for heavy computations on the full dynamic problem, provide insight into how structural damping and external loading affect shunt tuning and better describe the effective dynamic capacitance, evaluated as the frequency dependent charge-to-voltage ratio.

Keywords:

Resonant piezoelectric shunt damping, Residual mode correction, Effective electromechanical coupling coefficient, Structural damping, Arbitrary load, Frequency response analysis

1. Introduction

Excessive vibrations of flexible structures may be mitigated by use of piezoelectric materials wired to an electric network (shunt). The piezoelectric shunt can be designed as an active, semi-active or passive system. The active shunt requires a constant power supply and active control of e.g. a negative capacitance [1, 2, 3, 4], switches [5] or a feedback system [6, 7], while the semi-active shunt relies less on sophisticated control systems and therefore theoretically more equivalent to a passive shunt. Examples of the latter are passive switching techniques [8] or the use of synthetic inductors [9, 10], which traditionally have been added to overcome challenges associated with passive inductors at high Henry values. Recently, large passive inductances have been realized by winding

*Corresponding author
Email address: jotof@mek.dtu.dk (Johan Frederik Toftekær)

a copper wire around a magnetic core [11], paving the way for the design of fully passive inductive-resistive (LR) shunts [12, 13]. Alternatively, programmable digital shunts with micro-controller units [9, 14] may be used to synthesize the desired shunt impedance, permitting the construction of very precise linear and non-linear shunts [15]. The prospects for a precise digital shunt have increased the relevance of an accurate description of the structural dynamics of flexible structures with shunted piezoelectric materials (electromechanical structures), as this may lead to significant improvements of the shunt damping efficiency.

The most commonly used piezoelectric shunt contains an inductance (L) and a resistance (R) wired in parallel or series with the piezoelectric material. The shunted piezoelectric material hereby acts as a resonant vibration absorber with stiffness, inertia and damping defined by the inherent piezoelectric capacitance (C_p), shunt inductance and resistance, respectively. Piezoelectric LR-shunt damping was initially proposed and experimentally demonstrated by Forward [16], while tuning principles for the series [17], parallel [18] and multi-branch [19] shunts were derived subsequently. Numerous shunt tuning principles [20, 10, 21, 22] have since been proposed and compared [23, 24], although in most cases only vaguely verified by experiments. This may be due to the fact that most initial shunt tuning principles have been based on inaccurate modal truncations of the electromechanical structure. Recently, more accurate modal truncation models [25, 26] and tuning methods with corrections for non-resonant vibration modes [27, 28, 29] have been proposed, leading to a better understanding and evaluation of the effective modal capacitance used in piezoelectric shunt tuning. Subsequently, methods using available experimental data for the evaluation of the modal capacitance [13] have been proposed, permitting the derivation of shunt tuning methods that are less vulnerable to inconsistencies between the numerical models and their underlying real-life structures. Nonetheless, some factors, such as structural damping and external loads, are still neglected, and precise explicit frequency response functions (FRFs) for an electromechanical structure have not been derived.

A shunted piezoelectric material attached to a flexible structure acts as a local damper, whereby the resulting damping of the structure becomes non-orthogonal, prohibiting the structural response to be evaluated by standard modal truncation methods. Furthermore, it is undesirable to evaluate the full complex eigenvalue problem of the electromechanical structure, as this may be very cumbersome even for fairly small numerical models. Instead, a precise description of the structural response may be obtained by an interpolation between two limiting eigenvalue problems. In [30] the interpolation between an undamped and a constrained eigenvalue problem was used to determine the

optimum tuning, sizing and placement of local viscous dampers. In the case of piezoelectric shunt damping the limiting eigenvalue problems are associated with short- (SC) and open circuiting (OC) of the piezoelectric electrodes [29], where the shift from SC to OC increases the apparent stiffness of the piezoelectric material. The principle of interpolating between the SC and OC eigenvalue problems was used in [26] to establish a combined modal truncation, which accurately determines the frequency response around the resonant frequency targeted by the piezoelectric shunt. Additionally, a truncation method based on the eigenvalue problem associated with pure L-shunts were proposed, which is not considered in the present paper, as this strategy requires prior tuning of the inductance, implying an extra eigenvalue problem or additional experimental measurements. However, explicit FRFs were not derived in [26] and a Gram-Smith algorithm had to be applied in order to obtain an accurate frequency response around higher vibration modes. In [29] the combined modal truncation with SC and OC mode shapes was further used to derive optimum piezoelectric LR-shunt tuning and an alternative expression for the effective electromechanical coupling coefficient (EMCC) [31].

In the present paper, the idea of interpolating between the SC and OC eigenvalue problems from [26] is used to derive precise explicit FRFs for the mechanical displacements and the electrical charge and voltage around a resonant vibration mode of a moderately damped structure targeted by a piezoelectric shunt. Subsequently, it is demonstrated how these explicit expressions permit the derivation of an equivalent dynamic capacitance [32, 2, 7, 3] and the development of shunt tuning methods, which account for structural damping [22] and external load acting on the structure. The explicit FRFs and proposed piezoelectric shunt tuning methods are verified by a numerical analysis of a cantilever benchmark beam with experimental data available in e.g. [10, 26]. The proposed explicit modal truncation method and tuning principles are highly applicable to other types of vibration absorbers, and may constitute the basis for further developments and the inclusion of more distinct structural properties, such as intrinsic resistance in the piezoelectric material [33] or temperature [34] and frequency dependencies of the piezoelectric permittivity. Finally, the explicit format of the derived FRFs permit the development of new shunt tuning methods based on objectives different from those considered in the present paper.

2. Discretized Vibration Problem

A moderately damped structure (damping ratio $\zeta_r \leq 0.05$) with an attached and shunted piezoelectric material (Figure 1) may be discretized by finite elements [28], whereby the vibration prob-

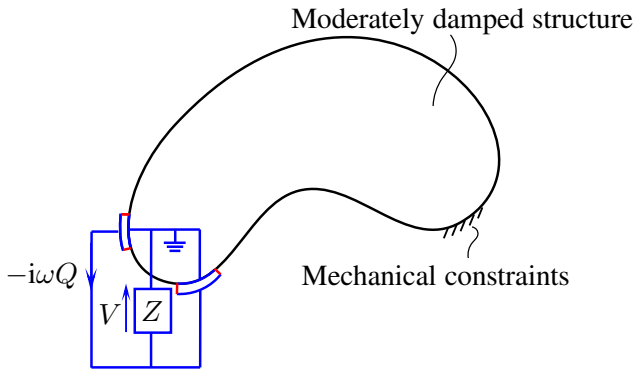

Figure 1: Moderately damped structure with a shunted piezoelectric material.

lem can be written as

$$\begin{aligned} \left(\mathbf{K} + \mathrm{i}\omega\mathbf{C} - \omega^2\mathbf{M}\right)\mathbf{u} + \mathbf{k}_{me}V &= \mathbf{f} \\ \mathbf{k}_{me}^T\mathbf{u} - C_pV &= -Q \end{aligned} \tag{1}$$

when harmonic solutions $\boldsymbol{u} = \mathbf{u}\exp(\mathrm{i}\omega t)$ and loading $\boldsymbol{f} = \mathbf{f}\exp(\mathrm{i}\omega t)$ are assumed, with angular frequency ω, time t and imaginary unit $\mathrm{i} = \sqrt{-1}$. Furthermore, one of the piezoelectric electrodes is considered to be grounded, whereby the charge Q and voltage V are quantities in the non-grounded electric degree of freedom (dof) [36]. The stiffness $\mathbf{K}$, mass $\mathbf{M}$ and damping $\mathbf{C}$ matrices describe the mechanical properties, while the vector $\mathbf{k}_{me}$ governs the coupling with the electric domain, characterized in (1) by the blocked piezoelectric capacitance C_p. A thorough review of finite element techniques for modelling of piezoelectric structural elements is provided in [35].

The relation between the charge Q and voltage V in (1) depends on the electric circuit (or shunt), connecting the piezoelectric electrodes. It may be described by the impedance relation

$$V = -\mathrm{i}\omega Z(\omega)Q \tag{2}$$

with shunt impedance $Z(\omega)$. In the limits $Z(\omega) \to 0$ and $Z(\omega) \to \infty$, the equations in (1) define respectively the SC and OC eigenvalue problems

$$\left(\mathbf{K} - \omega_j^2\mathbf{M}\right)\mathbf{u}_j = \mathbf{0} \quad , \quad \left(\mathbf{K} + \frac{1}{C_p}\mathbf{k}_{me}\mathbf{k}_{me}^T - \hat{\omega}_j^2\mathbf{M}\right)\hat{\mathbf{u}}_j = \mathbf{0} \tag{3}$$

determining the SC and OC frequencies (ω_j and $\hat{\omega}_j$) and the corresponding mode shape vectors ($\mathbf{u}_j$ and $\hat{\mathbf{u}}_j$) for a vibration mode j. The mode shapes are normalized to unit modal mass such that the following relations are valid,

$$\begin{aligned} k_j = \mathbf{u}_j^T\mathbf{K}\mathbf{u}_j = \omega_j^2 \quad , \quad m_j = \mathbf{u}_j^T\mathbf{M}\mathbf{u}_j = 1 \\ \hat{k}_j = \hat{\mathbf{u}}_j^T\left(\mathbf{K} + \frac{1}{C_p}\mathbf{k}_{me}\mathbf{k}_{me}^T\right)\hat{\mathbf{u}}_j = \hat{\omega}_j^2 \quad , \quad \hat{m}_j = \hat{\mathbf{u}}_j^T\mathbf{M}\hat{\mathbf{u}}_j = 1 \end{aligned} \tag{4}$$

The electric equation in (1) may additionally be used to determine an SC modal charge Q_j and OC modal voltage $\hat{V}_j$,

$$Q_j = -\mathbf{k}_{me}^T \mathbf{u}_j \quad , \quad \hat{V}_j = \frac{1}{C_p} \mathbf{k}_{me}^T \hat{\mathbf{u}}_j \tag{5}$$

Their ratio then provides a so-called modal capacitance

$$C_j = -\frac{Q_j}{\hat{V}_j} \tag{6}$$

which in [29] has been found to accurately estimates a characteristic capacitance of the piezoelectric material for a specific vibration mode j. The solutions to the SC and OC eigenvalue problems also quantify the electromechanical coupling for a vibration mode j by the co-called effective EMCC

$$\kappa_j^2 = \frac{\hat{\omega}_j^2 - \omega_j^2}{\omega_j^2} = -\frac{Q_j \hat{V}_j}{\tilde{m}_j \omega_j^2} \tag{7}$$

which may alternatively be determined from the modal SC charge Q_j, OC voltage $\hat{V}_j$ and an intermediate modal mass

$$\tilde{m}_j = \mathbf{u}_j^T \mathbf{M} \hat{\mathbf{u}}_j = -\frac{Q_j \hat{V}_j}{\hat{\omega}_j^2 - \omega_j^2} \simeq 1 \tag{8}$$

that in most cases approximately equals unity, as the difference between the SC and OC mode shapes is often very limited [29]. In the following sections it is demonstrated how the full vibration problem (1) can be reduced by introducing a combined modal truncation with the SC and OC mode shapes in order to obtain an explicit solution format for the shunt tuning and frequency response around the resonant vibration mode $j = r$ targeted by the piezoelectric shunt.

3. Response to modal load

In this section the structure is considered to be excited by a modal load $\mathbf{f} = \mathbf{M}\mathbf{u}_r$ distributed according to the deformation pattern of the SC target vibration mode r, whereby the dynamic response is dominated by this vibration mode. However, when the piezoelectric shunt is introduced neither a truncation with SC or OC mode shapes can fully represent the dynamics of the system, since the response will be associated with an intermediate complex eigenvalue problem. Instead of evaluating the complex eigenvalue problem, a combined modal truncation with both the SC and OC mode shapes is therefore introduced for the target mode r as

$$\mathbf{u} = \mathbf{u}_r r_r + \hat{\mathbf{u}}_r \hat{r}_r = [\mathbf{u}_r \ \hat{\mathbf{u}}_r] \begin{bmatrix} r_r \ \hat{r}_r \end{bmatrix}^T = \tilde{\mathbf{U}}_r \tilde{\mathbf{r}}_r \tag{9}$$

By introducing this combined modal truncation, the vibration problem (1) may be written as

$$\begin{aligned} \tilde{\mathbf{U}}_r^T \left(\mathbf{K} + \mathrm{i}\omega \mathbf{C} - \omega^2 \mathbf{M} \right) \tilde{\mathbf{U}}_r \tilde{\mathbf{r}}_r + \tilde{\mathbf{U}}_r^T \mathbf{k}_{me} V &= \tilde{\mathbf{U}}_r^T \mathbf{f} \\ \mathbf{k}_{me}^T \tilde{\mathbf{U}}_r \tilde{\mathbf{r}}_r - C_p V &= -Q \end{aligned} \tag{10}$$

when pre-multiplied by $\tilde{\mathbf{U}}_r$. When orthogonal structural damping is assumed, e.g. Rayleigh damping, and upon division with the intermediate modal mass (8), which is subsequently replaced by unity according to (8), the modal equations in (10) may be written in matrix form as

$$\begin{bmatrix} \omega_r^2 - \omega^2 + 2\mathrm{i}\zeta_r\omega_r\omega & \omega_r^2 - \omega^2 + 2\mathrm{i}\zeta_r\omega_r\omega & -Q_r \\ \omega_r^2 - \omega^2 + 2\mathrm{i}\zeta_r\omega_r\omega & \omega_r^2 - \omega^2 + 2\mathrm{i}\zeta_r\omega_r\omega - Q_r\hat{V}_r\left(1 - \frac{C_p}{C_r}\right) & -Q_r\frac{C_p}{C_r} \\ \hat{V}_r C_r & \hat{V}_r C_p & -C_p \end{bmatrix} \begin{bmatrix} r_r \\ \hat{r}_r \\ V \end{bmatrix} = \begin{bmatrix} f_r \\ \hat{f}_r \\ -Q \end{bmatrix} \tag{11}$$

where $2\zeta_r\omega_r = c_r/m_r$ defines the SC modal damping ratio ζ_r, while $f_r = \mathbf{u}_r^T\mathbf{f}$ and $\hat{f}_r = \hat{\mathbf{u}}_r^T\mathbf{f}$ are the SC and OC modal loads, respectively. Next, the charge Q in the last equation of (11) is eliminated by the impedance relation (2), whereby it can be written as

$$\hat{V}_r r_r + \hat{V}_r\frac{C_p}{C_r}\hat{r}_r = \underbrace{\left(\frac{C_p}{C_r} + Y_r(\omega)\right)}_{G_r(\omega)} V \tag{12}$$

defining the normalized admittance function $Y_r(\omega)$ as

$$Y_r(\omega) = \frac{1}{\mathrm{i}\omega Z(\omega) C_r} \tag{13}$$

The system of modal equations (11) may then be reduced to

$$\begin{bmatrix} X_r(\omega)G_r(\omega) - Q_r\hat{V}_r & X_r(\omega)G_r(\omega) - Q_r\hat{V}_r\frac{C_p}{C_r} \\ X_r(\omega)G_r(\omega) - Q_r\hat{V}_r\frac{C_p}{C_r} & \left(X_r(\omega) - Q_r\hat{V}_r\right)G_r(\omega) + Q_r\hat{V}_r\frac{C_p}{C_r}Y_r(\omega) \end{bmatrix} \begin{bmatrix} r_r \\ \hat{r}_r \end{bmatrix} = \begin{bmatrix} f_r G_r(\omega) \\ \hat{f}_r G_r(\omega) \end{bmatrix} \tag{14}$$

by eliminating the shunt voltage V using (12) and introducing

$$X_r(\omega) = \omega_r^2 - \omega^2 + 2\mathrm{i}\zeta_r\omega_r\omega \tag{15}$$

as the frequency function for the basic mode r vibration problem. The determinant of the modal system matrix in (14) is given by

$$-Q_r\hat{V}_r\left(1 - \frac{C_p}{C_r}\right)G_r(\omega)\left[X_r(\omega)\left(1 + Y_r\left(\omega\right)\right) - Q_r\hat{V}_r\right] \tag{16}$$

The expression in the square brackets of (16) thereby defines the characteristic polynomial

$$P_r(\omega) = \left(\omega_r^2 - \omega^2 + 2\mathrm{i}\zeta_r\omega_r\omega\right)\left(1 + \frac{1}{\mathrm{i}\omega Z(\omega) C_r}\right) - Q_r\hat{V}_r \tag{17}$$

of the dynamic system in (14). This characteristic polynomial is identical to that derived in [29] and the present approach therefore provides an alternative derivation path to the shunt tuning method suggested there. The benefit of the present approach is however that it provides the coupled modal

equations in (14), from which explicit expressions for the modal coefficients, valid around the target vibration mode r, can be derived as

$$\begin{aligned} r_r &= \frac{Y_r(\omega)}{P_r(\omega)} f_r - \left(\frac{X_r(\omega) Y_r(\omega)}{P_r(\omega)} + \frac{C_p}{\Delta C_r} \right) \frac{f_r - \hat{f}_r}{Q_r \hat{V}_r} \\ \hat{r}_r &= \frac{1}{P_r(\omega)} \hat{f}_r + \left(\frac{X_r(\omega) Y_r(\omega)}{P_r(\omega)} + \frac{C_p}{\Delta C_r} \right) \frac{f_r - \hat{f}_r}{Q_r \hat{V}_r} \end{aligned} \tag{18}$$

with $\Delta C_r = C_r - C_p$ being the correction in modal capacitance. It is seen that the second term for both modal coefficients in (18) vanishes when $f_r \simeq \hat{f}_r$, in which case the frequency response for the mechanical displacements (9) can be determined by

$$\mathbf{u} = \mathbf{u}_r \frac{Y_r(\omega)}{P_r(\omega)} f_r + \hat{\mathbf{u}}_r \frac{1}{P_r(\omega)} \hat{f}_r \tag{19}$$

The corresponding frequency response for the shunt voltage can further be found by inserting the modal coefficients (18) into (12), yielding the voltage FRF

$$\frac{V Q_r}{f_r} = \frac{1}{P_r(\omega)} \left[Q_r \hat{V}_r - X_r(\omega) \left(1 - \frac{\hat{f}_r}{f_r} \right) \right] \tag{20}$$

normalized by the modal charge Q_r and SC modal load f_r. Again, it is seen that the second term in (20) vanishes when $f_r \simeq \hat{f}_r$. Similarly, the charge FRF may be obtained from (12) when the voltage V is eliminated in terms of Q by the impedance relation (2). After inserting the modal coefficients (18), the charge FRF is then given by

$$\frac{Q \hat{V}_r}{f_r} = \frac{Y_r(\omega)}{P_r(\omega)} \left[Q_r \hat{V}_r - X_r(\omega) \left(1 - \frac{\hat{f}_r}{f_r} \right) \right] \tag{21}$$

when normalized by the OC modal voltage $\hat{V}_r$ and SC modal load f_r. The ratio $(-Q/V)$ between the charge (21) and voltage (20) is hereby found to consistently recover the impedance relation (2).

4. Response to arbitrary load

In the previous section, it has been assumed that the external load on the structure is spatially distributed as not to excite other modes ($j \neq r$) than the targeted vibration mode r. However, in the case of an arbitrary external load, the non-resonant vibration modes may influence the response around target mode r and they must therefore be accounted for in order to obtain a generally precise modal truncation.

The modal response for a specific vibration mode j is dominated by the modal stiffness and inertia for frequencies below and above the resonant frequency ω_j, respectively. In the present case,

the combined modal representation in (9) is therefore extended to account for both the SC dynamic influence from the modes below and the quasi-static influence from the modes above vibration mode $j = r$. A modal representation for the discrete displacements is hereby introduced as

$$\mathbf{u} = \underbrace{[\mathbf{U}\ \hat{\mathbf{u}}_r]}_{\tilde{\mathbf{U}}} \begin{bmatrix} \mathbf{r} \\ \hat{r}_r \end{bmatrix} + \sum_{j=r+1}^{n} \mathbf{u}_j r_j \simeq \sum_{j=1}^{r-1} \mathbf{u}_j r_j + \mathbf{u}_r r_r + \hat{\mathbf{u}}_r \hat{r}_r + \mathbf{u}_s \tag{22}$$

where the matrix $\mathbf{U} = [\mathbf{u}_1 \dots \mathbf{u}_r]$ contains the SC mode shapes for $j \leq r$ as columns with $\mathbf{r} = [\mathbf{r}_j^T\ r_r]^T = [r_1 \dots r_r]^T$ as the associated modal coefficients. In the combined modal truncation proposed in [26], the vibration modes below the target mode have been represented by a truncation with both the SC and OC mode shapes, whereby a Gram-Smith algorithm has been applied to obtain orthogonal eigenvectors. However, when the piezoelectric shunt targets vibration mode r, the influence from the lower vibration modes is accurately represented by the pure SC truncation as the impedance function for an optimum tuning to mode r at lower frequencies approaches zero [29].

The quasi-static contribution from the vibration modes above target mode r in the last term of (22) is obtained by subtracting the modal response of modes $j = 1 \dots r$ from the full static solution

$$\mathbf{u}_s = \left(\mathbf{K}^{-1} - \tilde{\mathbf{U}} \left(\tilde{\mathbf{U}}^T \mathbf{K} \tilde{\mathbf{U}} \right)^{-1} \tilde{\mathbf{U}}^T \right) \mathbf{f} \tag{23}$$

The dynamic part of the response is determined from the modal reduced vibration problem for modes $j = 1 \dots r$, which can be written as

$$\begin{bmatrix} \mathbf{X}_j(\omega) & 0 & \mathbf{X}_j(\omega)\tilde{\mathbf{m}}_{j,r} & -\mathbf{Q}_j^T \\ 0 & X_r(\omega) & X_r(\omega) & Q_r \\ \tilde{\mathbf{m}}_{j,r}^T \mathbf{X}_j(\omega) & X_r(\omega) & X_r(\omega) - Q_r \hat{V}_r \left(1 - \frac{C_p}{C_r}\right) & -Q_r \frac{C_p}{C_r} \\ \hat{\boldsymbol{V}}_j \mathbf{C}_j & \hat{V}_r C_r & \hat{V}_r C_p & -C_p \end{bmatrix} \begin{bmatrix} \mathbf{r}_j \\ r_r \\ \hat{r}_r \\ V \end{bmatrix} = \begin{bmatrix} \mathbf{U}_j^T \mathbf{f} \\ \mathbf{u}_r^T \mathbf{f} \\ \hat{\mathbf{u}}_r^T \mathbf{f} \\ -Q \end{bmatrix} \tag{24}$$

when the mechanical vibration problems for mode $j = 1 \dots r-1$ are collected in the diagonal matrix

$$\mathbf{X}_j(\omega) = \begin{bmatrix} X_1(\omega) & & \\ & \ddots & \\ & & X_{r-1}(\omega) \end{bmatrix} \tag{25}$$

with $X_j(\omega)$ defined as in (15). It is seen from (24) that the modal equations for the lower modes $j = 1 \dots r-1$ couple with the OC modal equation for mode r via the intermediate modal mass vector $\tilde{\mathbf{m}}_{j,r}$, which does not vanish as the corresponding SC and OC mode shapes are not entirely orthogonal. This intermediate modal mass may be determined for each mode j with respect to the

OC mode r according to (8) as

$$\tilde{\mathbf{m}}_{j,r} = [\tilde{m}_{1,r} \ \dots \ \tilde{m}_{r-1,r}]^T \quad , \quad \tilde{m}_{j,r} = \mathbf{u}_j^T \mathbf{M} \hat{\mathbf{u}}_r = -\frac{Q_j \hat{V}_r}{\hat{\omega}_r^2 - \omega_j^2} \simeq \frac{Q_j \hat{V}_r}{X_j(\omega)} \tag{26}$$

where the last convenient approximation is valid for frequencies in close proximity to the target OC frequency $\omega \simeq \hat{\omega}_r$. This intermediate modal mass (26) is now used in each modal equation for mode $j = 1 \dots r-1$, whereby the modal coefficients in $\mathbf{r}_j$ can be obtained as

$$r_j = -\frac{Q_j \hat{V}_r}{X_j(\omega)} \hat{r}_r + \frac{Q_j}{X_j(\omega)} V + \frac{1}{X_j(\omega)} f_j \tag{27}$$

When inserting the modal coefficients r_j, the two last equations of (24) can be written as

$$X_r(\omega) r_r + \left[X_r(\omega) - Q_r \hat{V}_r \left(1 - \frac{C_p'(\omega)}{C_r} \right) \right] \hat{r}_r - Q_r \frac{C_p'(\omega)}{C_r} V = \hat{f}_r - Q_r \sum_{j=1}^{r-1} \frac{\hat{V}_j}{X_j(\omega)} \frac{C_j}{C_r} f_j \tag{28a}$$

$$\hat{V}_r r_r + \hat{V}_r \frac{C_p'(\omega)}{C_r} \hat{r}_r + \sum_{j=1}^{r-1} \frac{\hat{V}_j}{X_j(\omega)} \frac{C_j}{C_r} f_j = \underbrace{\left(\frac{C_p'(\omega)}{C_r} + Y_r(\omega) \right)}_{\bar{G}_r(\omega)} V \tag{28b}$$

where the blocked capacitance

$$C_p'(\omega) = C_p - \sum_{j=1}^{r-1} \frac{Q_j \hat{V}_j}{X_j(\omega)} C_j \tag{29}$$

is altered by the influence from the vibration modes below target mode $j < r$. The shunt voltage V in (28b) is now inserted in the second SC equation of (24) and in the OC equation (28a), whereby the obtained reduced vibration problem,

$$\begin{bmatrix} X_r(\omega)\bar{G}_r(\omega) - Q_r \hat{V}_r & X_r(\omega)\bar{G}_r(\omega) - Q_r \hat{V}_r \dfrac{C_p'(\omega)}{C_r} \\ X_r(\omega)\bar{G}_r(\omega) - Q_r \hat{V}_r \dfrac{C_p'(\omega)}{C_r} & \left(X_r(\omega) - Q_r \hat{V}_r \right) \bar{G}_r(\omega) + Q_r \hat{V}_r \dfrac{C_p'(\omega)}{C_r} Y_r(\omega) \end{bmatrix} \begin{bmatrix} r_r \\ \\ \hat{r}_r \end{bmatrix} = \begin{bmatrix} f_r \bar{G}_r(\omega) + Q_r \displaystyle\sum_{j=1}^{r-1} \frac{\hat{V}_j}{X_j(\omega)} \frac{C_j}{C_r} f_j \\ \\ \hat{f}_r \bar{G}_r(\omega) - Q_r Y_r(\omega) \displaystyle\sum_{j=1}^{r-1} \frac{\hat{V}_j}{X_j(\omega)} \frac{C_j}{C_r} f_j \end{bmatrix} \tag{30}$$

only depends on the modal coefficients of target mode r. It can be seen that the left hand side system matrices in (30) and (14) are identical, except for the blocked capacitance, which for an arbitrary external load in (30) is replaced by the altered blocked capacitance $C_p'(\omega)$ defined in (29). The characteristic polynomial of (30) is therefore the same as for the modal load case and thus given by

(17). The modal coefficients in (30) then follow as

$$r_r = \frac{Y_r(\omega)}{P_r(\omega)} f_r - \left[\left(\frac{X_r(\omega) Y_r(\omega)}{P_r(\omega)} + \frac{C_p'(\omega)}{\Delta C_r(\omega)} \right) \frac{f_r - \hat{f}_r}{Q_r \hat{V}_r} + \sum_{j=1}^{r-1} \frac{C_j}{\Delta C_r(\omega)} \frac{V_j}{V_r} \frac{f_j}{X_j(\omega)} \right] \tag{31a}$$

$$\hat{r}_r = \frac{1}{P_r(\omega)} \hat{f}_r + \left[\left(\frac{X_r(\omega) Y_r(\omega)}{P_r(\omega)} + \frac{C_p'(\omega)}{\Delta C_r(\omega)} \right) \frac{f_r - \hat{f}_r}{Q_r \hat{V}_r} + \sum_{j=1}^{r-1} \frac{C_j}{\Delta C_r(\omega)} \frac{V_j}{V_r} \frac{f_j}{X_j(\omega)} \right] \tag{31b}$$

where $\Delta C_r(\omega) = C_r - C_p'(\omega)$ is a frequency dependent correction of the capacitance. The corresponding charge and voltage FRFs are found by inserting the modal coefficients (31) in the electric equation (28b), whereby it is found that the contributions from modes $j = 1 \ldots r-1$ cancel. Hereby, the same FRFs (20) and (21) as obtained for the modal load case are also valid in the present case with an arbitrary load distribution. Contrarily to the modal load case, the ratio between SC and OC modal loads may deviate from unity, whereby the second term in the square brackets of (20) and (21) will influence the voltage and charge frequency response.

The modal coefficients for mode $j = 1 \ldots r-1$ are found by inserting the OC modal coefficient (31b) and voltage (20) into (27), whereby r_j is determined by

$$r_j = \frac{f_j}{X_j(\omega)} - \frac{Q_j \hat{V}_r}{X_j(\omega)} \left[\left(\frac{X_r(\omega) Y_r(\omega)}{P_r(\omega)} + \frac{C_p'(\omega)}{\Delta C_r(\omega)} \right) \frac{f_r - \hat{f}_r}{Q_r \hat{V}_r} + \sum_{j=1}^{r-1} \frac{C_j}{\Delta C_r(\omega)} \frac{V_j}{V_r} \frac{f_j}{X_j(\omega)} \right] \tag{32}$$

The resulting displacements are then obtained by inserting these modal coefficients into (31), while (32) and the static deflection (23) are substituted into the modal representation (22). This yields an FRF given by

$$\mathbf{u} \simeq \sum_{j=1}^{r-1} \frac{\mathbf{u}_j f_j}{X_j(\omega)} + \frac{\mathbf{u}_r Y_r(\omega) f_r}{P_r(\omega)} + \frac{\hat{\mathbf{u}}_r \hat{f}_r}{P_r(\omega)} + \mathbf{u}_s - (\mathbf{u}_r - \hat{\mathbf{u}}_r) \left(\frac{X_r(\omega) Y_r(\omega)}{P_r(\omega)} + \frac{C_p}{\Delta C_r} \right) \frac{f_r - \hat{f}_r}{Q_r \hat{V}_r} \tag{33}$$

when the resonant frequencies are considered to be fairly separated, whereby terms with $1/X_j(\omega)$ in the square brackets of (31) and (32) vanish. The full FRF for the displacements is provided in Appendix A. It is furthermore seen that the last term in (33) in many cases will vanish because of the similar SC and OC modal loads ($f_r \simeq \hat{f}_r$) and mode shapes ($\mathbf{u}_r \simeq \hat{\mathbf{u}}_r$). However, the last term may influence the response at local dofs that are particularly affected by the shunted piezoelectric material.

5. Shunt tuning

The explicit FRFs for displacements, charge and voltage, account for structural damping and external load. Therefore, they permit the derivation of more generally applicable shunt tuning methods

with respect to a specific tuning objective and shunt configuration. A commonly applied objective for a parallel or series LR-shunt aims at obtaining two equal peaks in the frequency response curves for the mechanical displacements [21] or a fully flat plateau in the corresponding absorber response [37].

In the present case, the objective is based on the balanced calibration principle [37], that yields a flat absorber response, which for piezoelectric LR-shunt damping corresponds to a flat voltage response [29]. In [29] the tuning of parallel and series LR-shunts has been derived directly from the characteristic polynomial, which is identical to that in (17). However, as (17) is independent of both the structural damping and external load, a generally applicable shunt tuning procedures can not be obtained by this approach. Instead, the shunt tuning parameters will be derived by ensuring the desired flat plateau around the targeted natural frequency ω_r in the voltage response curve.

As demonstrated in [29, 13], the shunt damping performance is almost insensitive to small changes in the shunt resistance tuning, while it is highly sensitive to even minor alternations in the shunt inductance. The strategy of the present shunt tuning procedure is therefore to consider the shunt resistance tuning to be independent of the structural damping and external load, while the shunt inductance is tuned to obtain the flat voltage response by securing that the real part of the voltage derivative will vanish at the tuning frequency for target mode r. This approach is initially applied for the parallel LR-shunt, while an alternative tuning procedure for the series LR-shunt is instead based on a flat charge response, as this results in a simpler tuning format.

5.1. Parallel shunt tuning

The parallel LR-shunt, tuned according to the balanced calibration principle [37], results in a voltage response with a flat plateau at the target SC frequency ω_r [29]. However, when the targeted structure is exposed to an arbitrary external load and possesses inherent structural damping, this property may be compromised, causing higher peaks in the displacement frequency response. In the present approach, the inductance tuning is therefore altered in order to maintain a flat voltage response at the target SC frequency $\omega = \omega_r$ for any external load and structural damping of up to moderate magnitude. The shunt tuning is achieved by ensuring a zero real part in the corresponding derivative (with respect to ω) of the voltage response, which can be obtained from (20) as

$$\frac{V'(\omega)Q_r}{f_r} = -\frac{Q_r\hat{V}_r}{P_r^2(\omega)}\left[X_r'(\omega)\left(\frac{\hat{f}_r}{f_r}+Y_r(\omega)\right)+X_r(\omega)Y_r'(\omega)-\frac{X_r^2(\omega)Y_r'(\omega)}{Q_r\hat{V}_r}\left(1-\frac{\hat{f}_r}{f_r}\right)\right] \quad (34)$$

where the parallel LR-shunt admittance $Y_r(\omega)$ can be written as

$$Y_r(\omega) = -\left(\mathrm{i}\frac{\omega_r}{\omega}\rho_r + \frac{\omega_r^2}{\omega^2}\lambda_r\right) \quad (35)$$

by introducing

$$\rho_r = \frac{1}{\omega_r R C_r} \quad , \quad \lambda_r = \frac{1}{\omega_r^2 L C_r} \tag{36}$$

as non-dimensional resistance and inductance parameters, respectively. When inserting the admittance function (35) and the frequency function (15) into the voltage derivative (34), the solution at $\omega = \omega_r$ can be written as

$$\frac{V'(\omega_r) Q_r}{f_r} \simeq \frac{2\omega_r Q_r \hat{V}_r}{P_r^2(\omega)} \left[\frac{\hat{f}_r}{f_r} - \lambda_r - \mathrm{i} \left(\zeta_r \left(\frac{\hat{f}_r}{f_r} + \lambda_r \right) + \rho_r \right) \right] \tag{37}$$

by assuming that terms containing the factor $\zeta_r^2 (1 - \hat{f}_r / f_r) \to 0$ can be omitted for up to moderate values of structural damping (for example $\zeta_r \leq 0.05$). The full voltage derivative is provided in Appendix B. In order to determine the real part of (37), the (squared) characteristic polynomial $P_r(\omega)$ in the denominator is analyzed. By inserting the admittance function (35) in the characteristic polynomial (17), this can be written as

$$\frac{P_r(\omega_r)}{Q_r \hat{V}_r} = - \left(1 + \frac{2\zeta_r}{\kappa_r^2} \rho_r \right) - \frac{2\mathrm{i}\zeta_r}{\kappa_r^2} (1 - \lambda_r) \tag{38}$$

for $\omega = \omega_r$. The square of this characteristic polynomial is then obtained, simplifying to

$$\left(\frac{P_r(\omega_r)}{Q_r \hat{V}_r} \right)^2 \simeq \left(1 + \frac{2\zeta_r}{\kappa_r^2} \rho_r \right)^2 + \frac{4\mathrm{i}\zeta_r}{\kappa_r^2} \left(1 + \frac{2\zeta_r}{\kappa_r^2} \rho_r \right) (1 - \lambda_r) \tag{39}$$

as the factor $\zeta_r^2 (1 - \lambda_r)^2 \to 0$ when the normalized inductance λ_r is tuned to the SC frequency ω_r. The full expression for the squared characteristic polynomial is provided in Appendix B.

The real and imaginary parts of the voltage derivative (37) are now separated by multiplying and dividing (37) by the complex conjugate of the squared characteristic polynomial (39), see Appendix B, whereby the real part of the voltage derivative can be written as

$$\begin{aligned} \mathrm{Re} \left(\frac{V'(\omega_r) Q_r}{f_r} \right) \simeq \frac{2\omega_r (Q_r \hat{V}_r)^3}{P_r^2(\omega) \bar{P}_r^2(\omega)} \Bigg[& \left(1 + \frac{2\zeta_r}{\kappa_r^2} \rho_r \right)^2 \left(\frac{\hat{f}_r}{f_r} - \lambda_r \right) \\ & - \frac{4\zeta_r}{\kappa_r^2} \left(1 + \frac{2\zeta_r}{\kappa_r^2} \rho_r \right) (1 - \lambda_r) \left(\zeta_r \left(\frac{\hat{f}_r}{f_r} + \lambda_r \right) + \rho_r \right) \Bigg] \end{aligned} \tag{40}$$

which vanishes when the square bracket becomes zero. The optimum inductance tuning is thus obtained by solving for λ_r when the expression in the square brackets of (40) equals zero. This yields the non-dimensional inductance tuning

$$\frac{1}{\lambda_r} = \frac{1 - \dfrac{2\zeta_r}{\kappa_r^2} \rho_r}{\dfrac{\hat{f}_r}{f_r} - \dfrac{2\zeta_r}{\kappa_r^2} \left(2 - \dfrac{\hat{f}_r}{f_r} \right) \rho_r} \tag{41}$$

when it is assumed that the term multiplied by $\zeta_r^2(1-\lambda_r) \to 0$ can be omitted. It is seen from (41) that the original inductance tuning $1/\lambda_r = 1$ [29] is recovered in the case of a modal load ($f_r \simeq \hat{f}_r$), whereby the tuning will as well be independent of the structural damping. Contrarily, when the structure is exposed to an arbitrary load ($f_r \neq \hat{f}_r$), the structural damping alters the inductance tuning, reducing to $1/\lambda_r = f_r/\hat{f}_r$ for $\zeta_r \to 0$. In section 7 the accuracy of the inductance tuning (41) is analyzed and compared to the original tuning, in which loading and structural damping are unaccounted for.

5.2. Series shunt tuning

The series shunt tuning based on the balanced calibration principle [37] causes a flat plateau in the voltage frequency response at the tuning frequency $\omega = \hat{\omega}_r\sqrt{1+\kappa_r^2}$ [29]. However, as demonstrated next, a flat charge response as tuning objective will lead to simpler tuning expressions at the OC frequency $\hat{\omega}_r$. The charge FRF (21) may be written as

$$\frac{Q(\omega)\hat{V}_r}{f_r} = \frac{1}{\hat{P}_r(\omega)}\left[Q_r\hat{V}_r - X_r(\omega)\left(1-\frac{\hat{f}_r}{f_r}\right)\right] \tag{42}$$

after multiplying and dividing (21) with the normalized shunt impedance $Z_r(\omega) = \mathrm{i}\omega Z(\omega)C_r$. The altered characteristic polynomial $\hat{P}_r(\omega)$ in the denominator of (42) is then defined as

$$\hat{P}_r(\omega) = X_r(\omega)(1+Z_r(\omega)) - Q_r\hat{V}_r Z_r(\omega) = X_r(\omega) + \hat{X}_r(\omega)Z_r(\omega) \tag{43}$$

with the latter compact format obtained by introducing the OC frequency function

$$\hat{X}_r(\omega) = \hat{\omega}_r^2 - \omega^2 + 2\mathrm{i}\zeta_r\omega_r\omega \tag{44}$$

The derivative of the charge response function (42) may then be determined as

$$\begin{aligned}\frac{Q'(\omega)\hat{V}_r}{\hat{f}_r} = \frac{1}{\hat{P}_r^2(\omega)}\Bigg[&\hat{X}_r'(\omega)\left(\hat{X}_r(\omega)-X_r(\omega)\right)\left(\frac{f_r}{\hat{f}_r}+Z_r(\omega)\right)\\ &+\hat{X}_r(\omega)\left(\hat{X}_r(\omega)\frac{f_r}{\hat{f}_r}-X_r(\omega)\right)Z_r'(\omega)\Bigg]\end{aligned} \tag{45}$$

after inserting the altered characteristic polynomial (43) and its derivative, and subsequently using that $X_r'(\omega) = \hat{X}_r'(\omega)$. The normalized impedance $Z_r(\omega)$ for the series shunt can now be written as

$$Z_r(\omega) = \mathrm{i}\frac{\omega}{\hat{\omega}_r}\hat{\rho}_r - \frac{\omega^2}{\hat{\omega}_r^2}\hat{\lambda}_r \tag{46}$$

by introducing the non-dimensional resistance and inductance parameters

$$\hat{\rho}_r = \hat{\omega}_r RC_r \quad , \quad \hat{\lambda}_r = \hat{\omega}_r^2 LC_r \tag{47}$$

The charge derivative (45), evaluated at the target OC frequency $\hat{\omega}_r$, may then upon substitution of the normalized impedance (46) be written as

$$\frac{Q'(\hat{\omega}_r)\hat{V}_r}{\hat{f}_r} = \frac{2\hat{\omega}_r Q_r \hat{V}_r}{\hat{P}_r^2(\omega)} \left[\frac{f_r}{\hat{f}_r} - \hat{\lambda}_r + 2\zeta_r \frac{\omega_r}{\hat{\omega}_r}\hat{\rho}_r + \mathrm{i}\left(\hat{\rho}_r - \zeta_r \frac{\omega_r}{\hat{\omega}_r}\left(\frac{f_r}{\hat{f}_r} - 3\hat{\lambda}_r \right) \right) \right] \tag{48}$$

when omitting terms with $\zeta_r^2(1 - f_r/\hat{f}_r) \to 0$. The square of the altered characteristic polynomial (43) in the denominator of (48) is given by

$$\left(\frac{\hat{P}_r(\hat{\omega}_r)}{Q_r \hat{V}_r} \right)^2 \simeq \left(1 + \frac{2\zeta_r}{\kappa_r^2}\frac{\hat{\omega}_r}{\omega_r}\hat{\rho}_r \right)^2 - \frac{4\mathrm{i}\zeta_r}{\kappa_r^2}\frac{\hat{\omega}_r}{\omega_r}\left(1 + \frac{2\zeta_r}{\kappa_r^2}\frac{\hat{\omega}_r}{\omega_r}\hat{\rho}_r \right)(1 - \hat{\lambda}_r) \tag{49}$$

when $\hat{\lambda}_r$ is tuned to the target OC frequency $\hat{\omega}_r$, see Appendix C for the full expression. The real part of the charge derivative is then found by multiplying and dividing (48) by the conjugate $\bar{\hat{P}}_r^2(\omega)$ of the function in (49),

$$\begin{aligned} \mathrm{Re}\left(\frac{Q'(\hat{\omega}_r)\hat{V}_r}{\hat{f}_r} \right) \simeq & \frac{2\hat{\omega}_r (Q_r \hat{V}_r)^3}{\hat{P}_r^2(\omega)\bar{\hat{P}}_r^2(\omega)} \left[\left(1 + \frac{2\zeta_r}{\kappa_r^2}\frac{\hat{\omega}_r}{\omega_r}\hat{\rho}_r \right)^2 \left(\frac{f_r}{\hat{f}_r} - \hat{\lambda}_r + 2\zeta_r \frac{\omega_r}{\hat{\omega}_r}\hat{\rho}_r \right) \right. \\ & \left. - \frac{4\zeta_r}{\kappa_r^2}\frac{\hat{\omega}_r}{\omega_r}\left(1 + \frac{2\zeta_r}{\kappa_r^2}\frac{\hat{\omega}_r}{\omega_r}\hat{\rho}_r \right)(1 - \hat{\lambda}_r)\left(\hat{\rho}_r - \zeta_r \frac{\omega_r}{\hat{\omega}_r}\left(\frac{f_r}{\hat{f}_r} - 3\hat{\lambda}_r \right) \right) \right] \end{aligned} \tag{50}$$

The expression in the squared brackets must now equal zero in order to obtain the desired flat charge response at $\omega = \hat{\omega}_r$. When assuming a fixed resistance tuning, an optimum series inductance is obtained by

$$\hat{\lambda}_r \simeq \frac{\dfrac{f_r}{\hat{f}_r} + 2\zeta_r \dfrac{\omega_r}{\hat{\omega}_r}\hat{\rho}_r - \dfrac{2\zeta_r}{\kappa_r^2}\dfrac{\hat{\omega}_r}{\omega_r}\left(2 - \dfrac{f_r}{\hat{f}_r} \right)\hat{\rho}_r}{1 - \dfrac{2\zeta_r}{\kappa_r^2}\dfrac{\hat{\omega}_r}{\omega_r}\hat{\rho}_r} \tag{51}$$

when terms multiplied by ζ_r^2 are omitted. It is seen from (51) that in the case of a modal external load ($f_r \simeq \hat{f}_r$) and vanishing structural damping ($\zeta_r \to 0$) the shunt inductance tuning recovers the classic result $\hat{\lambda}_r = 1$, while the tuning is altered by the non-dimensional resistance for non-vanishing structural damping, even when the structure is excited by a modal load. As for the parallel inductance tuning, the series tuning reduces to the ratio $\hat{\lambda}_r = f_r/\hat{f}_r$ for an arbitrary external load when neglecting structural damping, although the full tuning formula (51) should be evaluated in the most general case with an arbitrary load and non-vanishing structural damping.

6. Equivalent dynamic capacitance

In [13] a piezoelectric shunt tuning method has been proposed based on experimental measurement signals of SC current and OC voltage over the piezoelectric electrodes. The method was

derived on the assumption of low structural damping and a load distribution that only excited the target vibration mode r. The modal capacitance C_r is then found to equal the ratio between the peak values in the frequency response for the SC charge (obtained from the measured current) and OC voltage. In the present approach, the derived explicit expressions for charge (21) and voltage (20) permit a more precise analysis of the modal capacitance and an equivalent dynamic capacitance around the target vibration mode r.

In section 3 the relation $-Q/V$ is found to recover the impedance relation (2). However, by considering the SC and OC limits of, respectively, the charge $\bar{Q}$ and voltage $\bar{V}$ amplitudes ($\bar{(\ )}$ refers to meassured values), the ratio $-\bar{Q}/\bar{V}$ can be found to provide an equivalent dynamic capacitance $\bar{C}(\omega)$ [32, 2, 7, 3].

In the SC and OC limits the admittance tends towards infinity $Y_r(\omega) \to \infty$ and zero $Y_r(\omega) \to 0$, respectively. Hereby, the SC charge $\bar{Q}$ and OC voltage $\bar{V}$ may be determined as

$$\frac{\bar{Q}}{f_r} = \frac{Q_r}{X_r(\omega)} \left[1 - \frac{X_r(\omega)}{Q_r \hat{V}_r} \left(1 - \frac{\hat{f}_r}{f_r} \right) \right] \quad , \quad \frac{\bar{V}}{f_r} = \frac{\hat{V}_r}{\hat{X}_r(\omega)} \left[1 - \frac{X_r(\omega)}{Q_r \hat{V}_r} \left(1 - \frac{\hat{f}_r}{f_r} \right) \right] \tag{52}$$

In Figure 2 these explicit FRFs for the SC charge and OC voltage are compared to the exact response obtained by evaluating the full vibration problem (1) with $V = 0$ and $Q = 0$, respectively. The frequency response is shown around the second vibration mode of a cantilever beam, used as well in the following numerical analysis in section 7. It is seen in Figure 2 that the SC charge and OC voltage have resonance peaks at the SC and OC frequencies, respectively. Furthermore, the explicit expressions in (52) (dashed curves) accurately estimate the exact solutions (solid curves) based on the full vibration problem (1). In the case of experimentally based shunt tuning these frequency response curves for the SC charge and OC voltage may be obtained as described in [13].

An explicit expression for the equivalent dynamic capacitance $\bar{C}(\omega)$ can now be obtained from the FRFs for SC charge and OC voltage (52) as

$$\bar{C}(\omega) = -\frac{\bar{Q}}{\bar{V}} = C_r \left(1 - \frac{Q_r \hat{V}_r}{\omega_r^2 - \omega^2 + 2\mathrm{i}\zeta_r \omega_r \omega} \right) \tag{53}$$

which is similar to the expression obtained in [3]. It is seen that the equivalent dynamic capacitance (53) is independent of the external load, but depends on the structural damping ζ_r, which may alter the evaluation of the modal capacitance C_r used for the piezoelectric shunt tuning. The equivalent dynamic capacitances, evaluated by the explicit expression (53) and from the charge and voltage response used in (1), are shown in Figure 3 by respectively the dashed and solid curves around the second resonant frequency of the cantilever beam analyzed in section 7. It can be seen that the

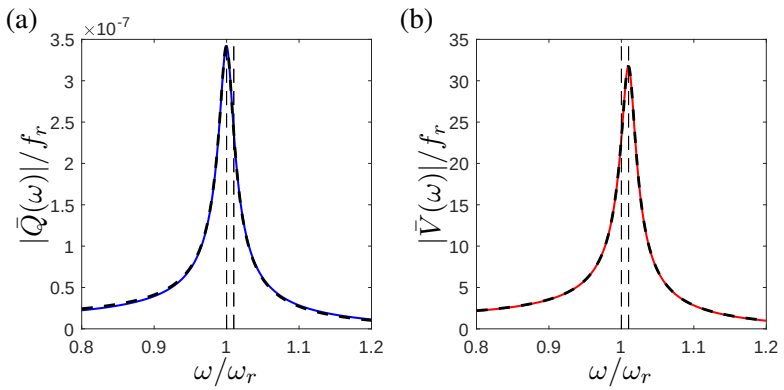

Figure 2: Frequency response for (a) SC charge and (b) OC voltage determined with the explicit expressions (52) (- -) and from the full vibration problem (1) (—,—). The vertical dashed lines indicates the SC and OC frequencies.

explicit (dashed curve) and exact (solid curve) capacitances are almost identical around a frequency between the SC and OC frequencies (vertical dashed lines). From (53) it can be found that for vanishing damping the absolute value of the equivalent capacitance in the SC and OC limits are given by

$$|\bar{C}(\omega_j)| = C_r \left| 1 - \frac{Q_r \hat{V}_r}{2\mathrm{i}\zeta_r \omega_r^2} \right| \to \infty, \quad |\bar{C}(\hat{\omega}_j)| = C_r \left| 1 - \frac{1}{1 + 2\mathrm{i}\zeta_r \frac{\omega_r \hat{\omega}_r}{Q_r \hat{V}_r}} \right| \to 0 \quad \text{for } \zeta_r \to 0 \tag{54}$$

while for a structural damping of $\zeta_r = 0.01$ the peaks (maximum and minimum) of the equivalent dynamic capacitance decrease and appear more separated. At frequencies well below and above the SC and OC frequencies, the equivalent dynamic capacitance is given by

$$\bar{C}(\omega \ll \omega_r) = C_r \left(1 + \kappa_r^2\right) = C_{r-1} \quad , \quad \bar{C}(\omega \gg \hat{\omega}_r^2) = C_r \tag{55}$$

as it can also be seen by the dashed curve in Figure 3(a), which approaches the horizontal dash-dotted (C_{r-1}) and solid (C_r) lines, respectively. For the solution based on the full vibration problem (1) (solid curve) in Figure 3(a) the presence of neighboring vibration modes is clearly seen to influence the equivalent dynamic capacitance. However, in the region between the SC and OC frequencies the explicit and exact dynamic capacitances are in good agreement and can be found to be independent of damping at an intermediate frequency (vertical dotted line in Figure 3) given by

$$\tilde{\omega}_r = \sqrt{\frac{\hat{\omega}_r^2 + \omega_r^2}{2}} = \sqrt{\omega_r^2 - \frac{Q_r \hat{V}_r}{2}} \tag{56}$$

At this frequency the absolute value of the equivalent dynamic capacitance can be determined as

$$|\bar{C}(\tilde{\omega}_r)| = C_r \left| \left(1 - \frac{Q_r \hat{V}_r}{Q_r \hat{V}_r/2 + 2\mathrm{i}\zeta_r \omega_r \tilde{\omega}_r} \right) \right| = C_r \tag{57}$$

which is seen to exactly recover the modal capacitance C_r. The detailed derivation of (57) is provided in Appendix D. One way to determine the modal capacitance C_r is therefore to measure the capacitance, e.g. with an impedancemeter [3], at the intermediate frequency $\tilde{\omega}_r$. However, as the curve in Figure 3 for the equivalent dynamic capacitance is relatively steep around the intermediate frequency $\tilde{\omega}_r$, a small error in the evaluation of $\tilde{\omega}_r$ will cause a substantial error on the measured modal capacitance. It may therefore be beneficial to apply the method of measuring the SC current and OC voltage as suggested in [13] and then to account for the influence from the structural damping using (53).

In [13] the SC modal charge Q_r and OC modal voltage $\hat{V}_r$ were estimated directly as the peak values in the frequency response for the SC charge $\bar{Q}$ and OC voltage $\bar{V}$ and then used to evaluate the modal capacitance C_r (6). However, when including the effect of structural damping and the arbitrary external loading, the relation between the measured peak SC charge to OC voltage ratio and the modal capacitance is slightly altered. Considering the frequency response for the SC charge and OC voltage in (52) the modal capacitance may be determined by

$$\bar{C}_r = -\frac{\bar{Q}(\omega_r)}{\bar{V}(\hat{\omega}_r)}\frac{f_r}{\hat{f}_r} = C_r\frac{\hat{\omega}_r}{\omega_r} \quad \Rightarrow \quad C_r = \bar{C}_r\frac{\omega_r}{\hat{\omega}_r}\frac{\hat{f}_r}{f_r} \tag{58}$$

when assuming that the structural damping ζ_r and external load acting on the structures are the same when the SC current (charge) and OC voltage are measured. For the detailed derivation of (58) see Appendix D. This means that the modal capacitance from [13] is altered by the SC to OC frequency ratio and the ratio between the OC and SC modal load, while the effect of structural damping vanishes, as it can be seen in Appendix D and (58). However, in most cases both the frequency and

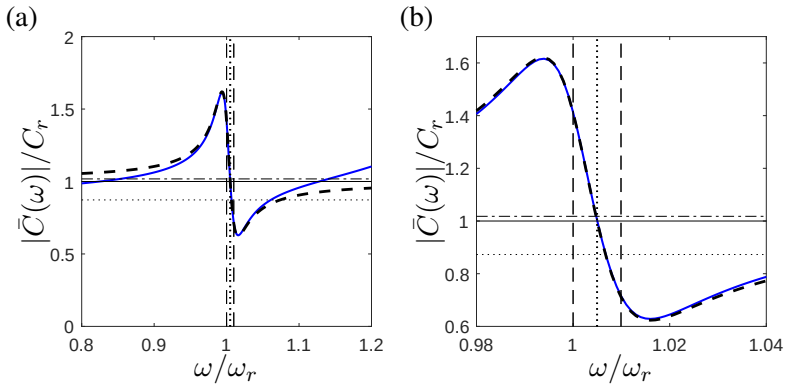

Figure 3: Explicit (53) (- - -) and exact (1) (—) equivalent capacitance around the second cantilever vibration frequency. The horizontal lines indicates the blocked (⋯) and modal capacitances C_r (—) and C_{r-1} (-·-), while the vertical lines provides the SC, intermediate and OC frequencies.

modal load ratios approach unity due to a limited influence from the shunted piezoelectric material on the resonant frequencies and mode shapes, in which cases the method described in [13] will be sufficient.

7. Numerical analysis

In the present section a numerical analysis of a cantilever beam (see Figure 4), previously analyzed in [10, 28, 26], is conducted in order to verify the derived explicit FRFs for the displacement, charge and voltage and to demonstrate the proposed piezoelectric shunt tuning method with correction for the specific external load and inherent structural damping. The dimensions of the cantilever beam and the attached piezoceramic patches can be seen in Figure 4, while the material properties are provided in Table 1. The structure is modeled in the plate-piezo FE-model developed in [28] with the beam discretized by 41×2 Kirchoff plate elements and each piezoceramic patch by 5×2 in-plane patch elements [28]. In the present analysis, the transverse inertia from the piezoceramic patches is included, whereby the SC and OC resonant frequencies for the three lowest flexural vibration modes in Table 2 are slightly lower than those provided in [28]. The corresponding three SC mode shapes are shown in Figure 5.

In the following, two loading scenarios are investigated. Initially, an external load $\mathbf{f} = \mathbf{M}\mathbf{u}_r$ proportioned to the deflection pattern of the target vibration mode r is considered, while secondly a point load p acts at the one third location from the fixed support (indicated by the arrows in Figure 5). In both cases a modal damping ratio $\zeta_r = 0.01$ is assumed and implemented in the numerical model as Rayleigh damping with $\alpha = \zeta_r \omega_r$ and $\beta = \zeta_r / \omega_r$. The optimum non-dimensional inductance tuning (41) and (51) is provided in Table 2 for the two load scenarios, while the parallel and series

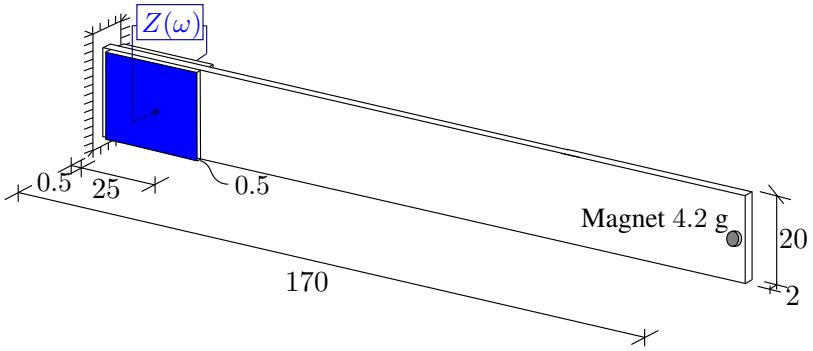

Figure 4: Dimensions in mm of cantilever beam and indication of the position of two collocated piezoceramic patches.

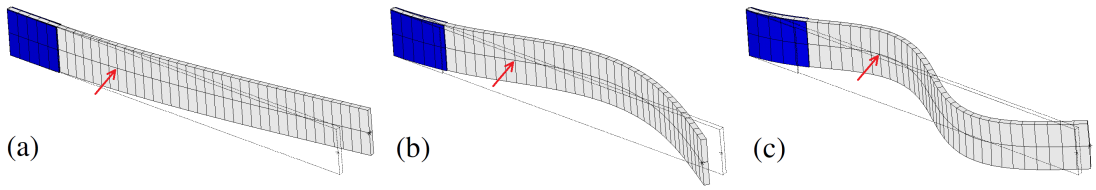

Figure 5: Flexural vibration mode 1-3 (a-c) for cantilever beam, red arrow indicates location of point load p.

resistance tuning in all cases can be found by

$$\frac{1}{\rho_r} = \hat{\rho}_r = \sqrt{2\kappa_r^2} \tag{59}$$

Table 2 shows that the inductance tuning for the modal load recovers the original tuning ($\lambda_r = 1$) for the parallel shunt, while the series inductance ($\hat{\lambda}_r$) is slightly altered by the structural damping in (51). In the point load scenario it is seen that both the parallel and series shunt inductances are significantly altered for modes 1 and 2. This is due to the applied point load p being located in a point of minor modal deflection for mode 1 and 2, consequently increasing the influence from the other non-resonant vibration modes. For mode 3 the point load p is located in a point of maximum modal deflection, whereby $f_r \simeq \hat{f}_r$ implies that the inductance tuning is similar to the original inductance tuning ($1/\lambda_r = \hat{\lambda}_r = 1$).

In the following subsections the explicit FRFs are compared to the exact response obtained with (1) for the two load scenarios and a parallel shunt configuration tuned to resonant vibration mode $r = 2$. Subsequently, both the parallel and series shunt tuning methods are analyzed for the two load scenarios and tuning to each of the three lowest vibration modes.

Table 1: Material properties for cantilever beam and piezoceramic patches.

	Beam		Piezo	
Density (kg/m^3)	ρ	2800	ρ_p	8500
Young's Modulus (GPa)	E	72	E_p	66.7
Poisson's ratio (-)	ν	0	ν_p	0
Piezoelectric coefficient (10^{-12}m/V)			d_{31}	-210
Blocked dielectric coefficient (F/m)			$\epsilon_{33}^{\varepsilon_p}$	$2068\varepsilon_0$

$\varepsilon_0 = 8.854 \times 10^{-12}$F/m [31]

Table 2: SC and OC frequencies, effective EMCC and modal capacitance for the three lowest flexural vibration modes, and non-dimensional inductance tuning in the case of a modal and a point load with a structural damping of $\zeta_r = 0.01$.

Mode	ω_r [rad/s]	$\hat{\omega}_r$ [rad/s]	κ_r^2 [%]	C_r [nF]		λ_r	$\hat{\lambda}_r$		λ_r	$\hat{\lambda}_r$
1	48.93	49.36	1.77	10.68	Modal load	1.000	1.005	Point load	0.960	1.046
2	336.6	340.0	1.99	10.49		1.000	1.005		0.977	1.029
3	947.9	956.3	1.77	10.29		1.000	1.005		0.999	1.006

7.1. Frequency response analysis - Modal load

It is now investigated how well the explicit FRFs for displacement (19), voltage (20) and charge (21) estimate the exact response obtained by evaluating the full discrete vibration problem (1) for each excitation frequency ω.

The frequency response for the cantilever tip displacement $|\tilde{u}_{tip}| = |u_{tip}|/(u_{r,tip} f_r/\omega_r^2)$ normalized by the tip deflection of the target mode shape $u_{r,tip}$ and the equivalent static deflection f_r/ω_r^2,

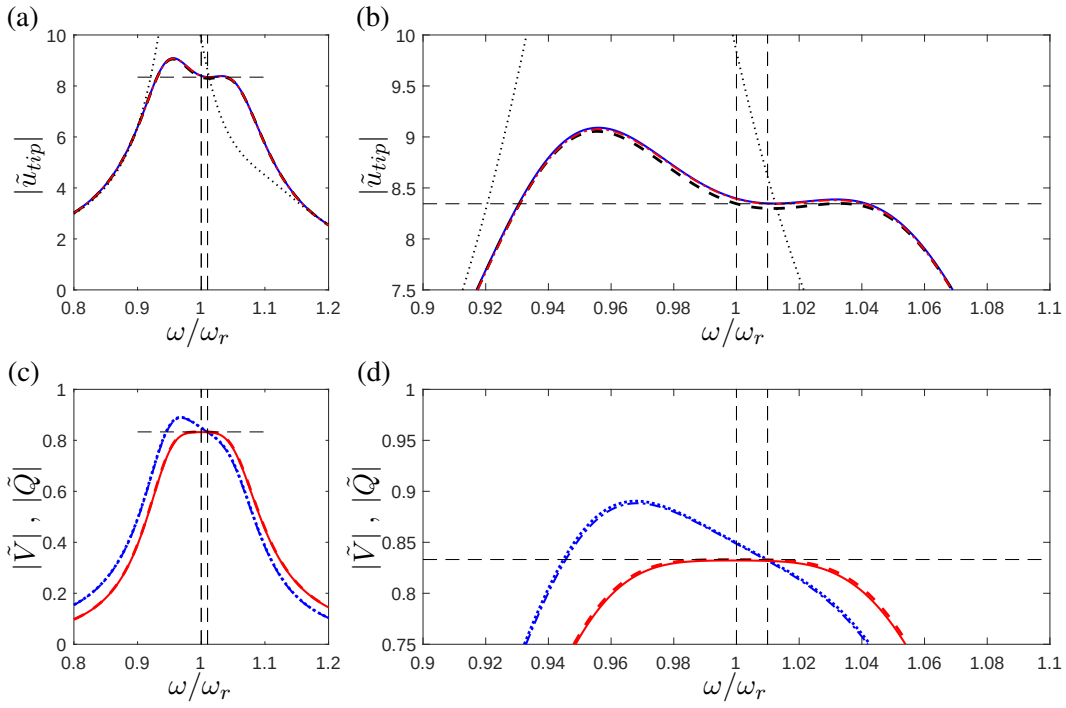

Figure 6: Frequency response to modal load for (a,b) the tip displacements and (c,d) charge and voltage around cantilever vibration mode $r = 2$. In (a,b) the frequency response are obtained from (1) (—), (10) (-··) and (19) (- -) and a pure SC modal truncation (···). In (c,d) the explicit charge (21) (···) and voltage (20) (- -) frequency response are compared to the exact charge (-··) and voltage (—) from (1). Dashed horizontal lines are in (a,b) $1/(2(\zeta_r+\zeta_d))$ and in (c,d) $\zeta_d/(\zeta_r+\zeta_d)$, while the vertical dashed lines indicate the SC and OC resonant frequencies.

obtained by (1) (solid curve) and (19) (dashed curve) are shown in Figure 6(a,b). The corresponding charge and voltage frequency response are further provided in Figure 6(c,d). It can be seen that the explicit solution (19) (dashed curve) in Figure 6(a,b) agrees with the exact response from (1) (solid curve), indicating that the combined modal truncation accurately captures the coupling between the SC and OC vibration modes caused by the piezoelectric shunt. Furthermore, it can be seen that by evaluating the reduced vibration problem (10) (red dash-dotted curve in Figure 6(a,b)) the exact frequency response is recovered even more accurately. It can hereby be deduced that the minor deviation observed in the explicit frequency response (19) (dashed curve in Figure 6(a,b)) is associated with the assumptions $\tilde{m}_r \simeq 1$ and $f_r \simeq \hat{f}_r$. It is further noted that the evaluation of the reduced vibration problem (10) corresponds to the combined modal reduction technique suggested in [26]. In any case, the frequency response in Figure 6(a,b) can be seen to have fairly flat plateaus around the target frequency $\omega = \omega_r$ at a level defined by the attainable damping ($\zeta_d = \sqrt{\frac{1}{8}\kappa_r^2}$, see [29]) and structural damping (ζ_r) by the relation

$$|\tilde{u}_{tip}(\omega_r)| = \frac{|u_{tip}(\omega_r)|}{u_{r,tip} f_r/\omega_r^2} = \frac{1}{2(\zeta_r + \zeta_d)} \tag{60}$$

obtained from the explicit FRF (19) at the SC frequency ω_r. The frequency response obtained by a pure SC modal truncation (dotted curves) is also provided in Figure 6(a,b), which shows that the single mode approximation leads to major deviations from the exact response calculation (solid curve). Figure 6(c,d) shows that the corresponding normalized voltage frequency response curves have a flat plateau at a level

$$|\tilde{V}(\omega_r)| = \frac{|V(\omega_r)|Q_r}{f_r} = \frac{\zeta_d}{\zeta_r + \zeta_d} \tag{61}$$

obtained from the explicit voltage FRF in (20). Furthermore, the explicit (20) (dashed curve) and exact (1) (solid curve) voltage frequency response $|\tilde{V}| = |V|Q_r/f_r$ in Figure 6(c,d) are seen to be almost identical. The same observation is made for the explicit (21) (dotted curve) and exact (1) (dash-dotted curve) normalized charge frequency response $|\tilde{Q}| = |Q|\hat{V}_r/f_r$. In the case of a parallel shunt tuning, the normalized charge response is seen to have a declining plateau around the target frequency $\omega = \omega_r$, intersecting the value $\zeta_d/(\zeta_r + \zeta_d)$ exactly at the OC frequency $\hat{\omega}_r$.

7.2. Frequency response analysis - Point load

The explicit FRFs for displacement (33), charge (21) and voltage (20) in the case of an arbitrary external load are now compared with the exact solutions obtained by evaluating the full vibration problem (1). As an example, the point load p in Figure 5 is applied to the structure, whereby the non-resonant vibration modes are expected to have an increased impact on the response, particularly

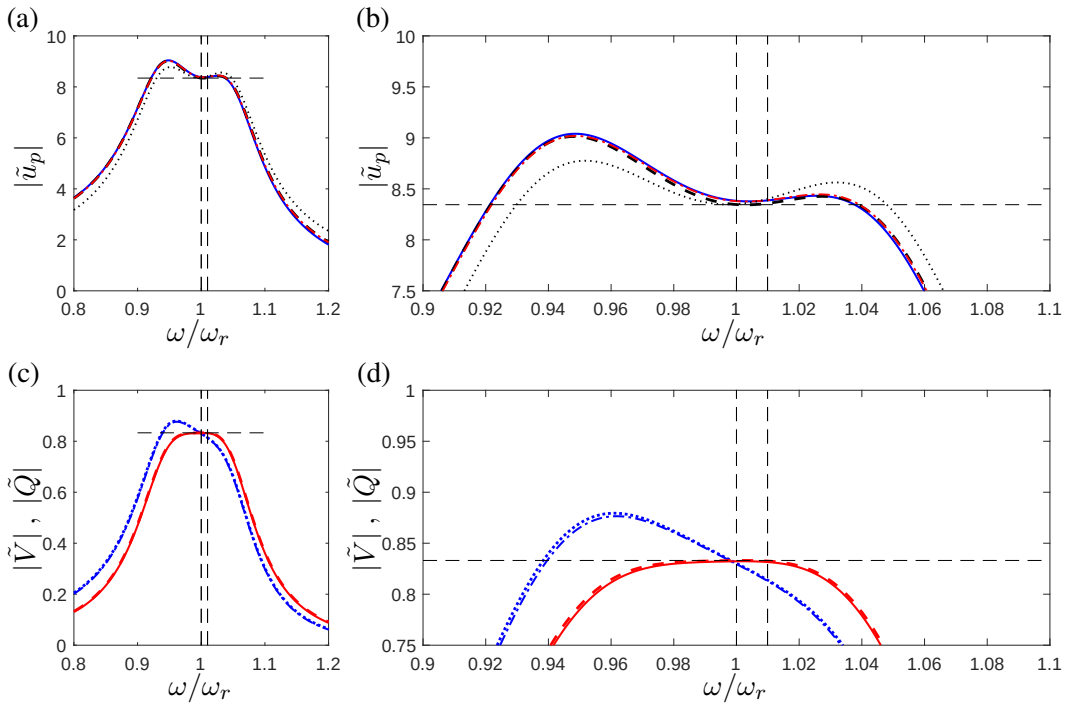

Figure 7: Frequency response to point load p for (a,b) displacements at p and (c,d) charge and voltage around cantilever vibration mode $r = 2$. In (a,b) the frequency response are obtained from (1) (—), (24) (- · -) and (33) (- -) and without correction for the non-resonant vibrations (19) (· · ·). In (c,d) the explicit charge (21) (· · ·) and voltage (20) (- -) frequency response are compared to the exact charge (- · -) and voltage (—) from (1). Dashed horizontal lines are in (a,b) $1/(2(\zeta_r + \zeta_d))$ and in (c,d) $\zeta_d/(\zeta_r + \zeta_d)$, while the vertical dashed lines indicate the SC and OC resonant frequencies.

around the resonant frequencies for the modes 1 and 2. The frequency response for the normalized displacements at the point load location $|\tilde{u}_p| = |u_p|/(u_{r,p} f_r/\omega_r^2)$ obtained with the explicit FRF (33) (dashed curve) and by the reduced (30) (dash-dotted curve) and full (1) (solid curve) vibration problems are shown in Figure 7(a,b) around the target mode $r = 2$. It can be seen that the three frequency response curves are very similar, while the omission of the influence from the non-resonant vibration modes (19) (dotted curve) in Figure 7(a,b) leads to deviations from the exact frequency response (solid curve). Furthermore, it can be seen in Figure 7(c,d) that the explicit charge and voltage frequency response (20) (dashed and dotted curves) agrees very well with the exact solution (1) (solid and dashed dotted curves) and that the voltage frequency response remains flat when the altered inductance tuning (41) is used. In the following subsection the importance of using the altered inductance tuning with correction for the structural damping and external load is investigated for both the parallel and series shunt configurations for a point load case.

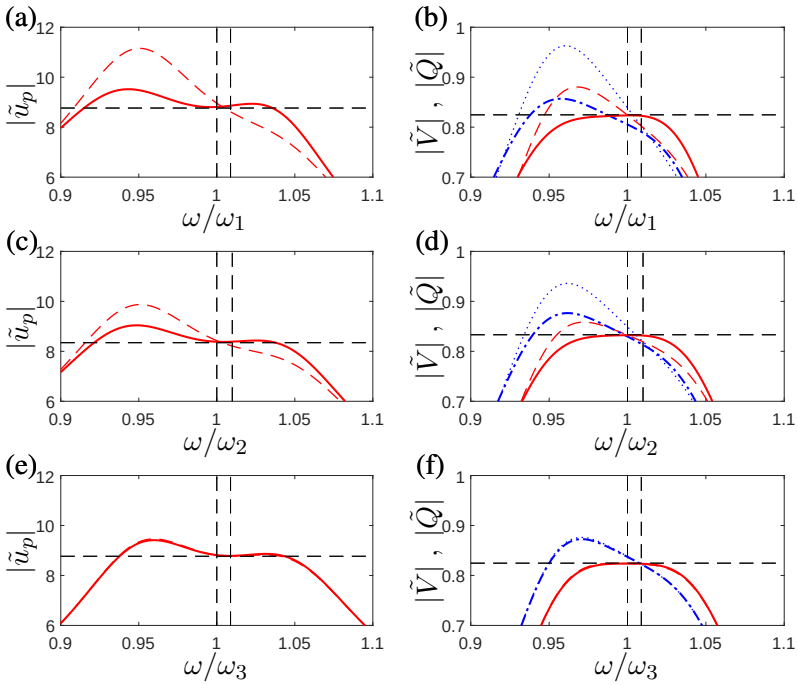

Figure 8: Frequency response to point load p and parallel shunt for (a,c,e) displacements at p and (b,d,f) charge and voltage around cantilever vibration mode 1-3. (a,c,e) shows the response for tuning with (—) and without (- -) correction for structural damping and external load and (b,d,f) the corresponding voltage (—,- -) and charge (-·-,···) response.

7.3. Shunt damping - Point load

In the case of a modal load, the altered inductance tuning (41) and (51) has, respectively, no and minor impact on the parallel and series shunts, as it can be seen in Table 2. The shunt damping performance to a modal load scenario is therefore not further investigated in the present paper. However, when an arbitrary external load excites the structure, the influence from the structural damping and external load on the inductance tuning increases, whereby the omission of these effects may lead to larger structural amplifications. When a point load p excites the cantilever at the one third position from the fixed support, the altered inductance tuning (41) and (51) provided in the last column of Table 2 is seen to deviate with 2-5% from the standard inductance tuning for vibration mode 1 and 2, while the tuning for mode 3 remains almost unchanged because the point load p is located at a modal maximum point. Figures 8(a,c,e) and 9(a,c,e) show the frequency response curves for the normalized displacements at the location of the point load $|\tilde{u}_p|$, for both the parallel and series shunts with inductances tuned with (solid curves) and without (dashed curves) correction for the structural damping and external load. It can be seen that the tuning without correction (dashed curves) causes

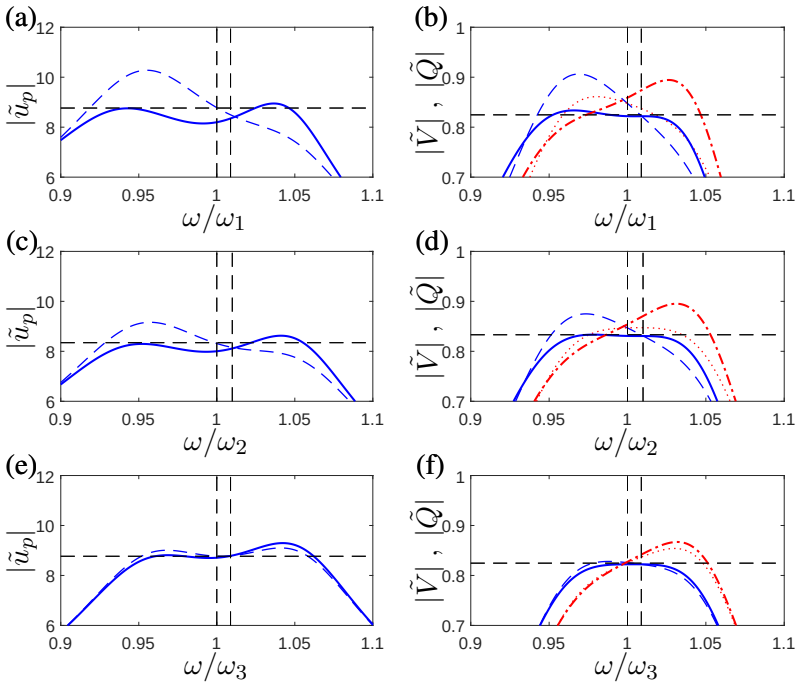

Figure 9: Frequency response to point load and series shunt for (a,c,e) displacements at point load and (b,d,f) charge and voltage around cantilever vibration mode 1-3. (a,c,e) shows the response for tuning with (—) and without (- -) correction for structural damping and external load and (b,d,f) the corresponding voltage (-·-,···) and charge (—,- -) response.

significantly larger amplifications around the first and second resonant frequencies for both shunts, while the effect of the correction is very limited for tuning to vibration mode 3. Furthermore, it can be seen that the tuning with correction (solid curves) in Figures 8(b,d,f) and 9(b,d,f) result in voltage and charge frequency response curves with flat plateaus at the tuning frequencies $\omega = \omega_r$ and $\hat{\omega}_r$ for the parallel and series shunts, respectively. Contrarily, the frequency response for the tuning without correction (dashed curves) in Figures 8(b,d,f) and 9(b,d,f) are not flat and have significant peaks for vibration modes 1 and 2. This shows that the altered inductance tuning for the parallel (41) and series shunts (51) successfully fulfill the desired flat plateau condition for the voltage and charge response, making the proposed shunt tuning method generally applicable and reliable for moderately damped structures with arbitrary dynamic loads.

8. Conclusion

Piezoelectric LR-shunt damping of inherently damped structures excited by arbitrary loads has been analyzed. The LR-shunt is considered to target a single resonant vibration mode, whereby the

dynamic response around the target frequency is associated with the solution of a complex eigenvalue problem. In order to avoid the expensive evaluation of this eigenvalue problem an interpolation (combined modal truncation) is therefore introduced between two limiting eigenvalue problems associated with SC and OC piezoelectric electrodes. When the load acting on the structure only excites the targeted vibration mode r, the combined modal truncation consistently reduces the vibration problem for the full flexible structure. In the case of an arbitrary excitation, it is found that the non-resonant vibration modes influence the response, whereby the combined modal truncation has been extended to include the SC dynamic and quasi-static contribution from, respectively the vibration modes below and above mode r. Explicit FRFs for the mechanical displacements and the electric charge and voltage are then derived by applying the modal truncation with contribution from the non-resonant vibration modes to the vibration problem for the full flexible structure.

The explicit FRFs for charge and voltage are subsequently used to derive an altered inductance tuning for the parallel and series shunts based on flat plateaus in the voltage and charge frequency response curves at the SC and OC frequencies, respectively. This tuning objective is inspired by the balanced calibration principle, originally proposed for the tuned mass damper, while alternative tuning principles with other objectives may be derived by considering the presented explicit FRFs. The proposed piezoelectric shunt tuning with correction for structural damping and the specific excitation load is verified by the analysis of a cantilever benchmark beam with numerical and experimental results available in the literature. It is shown that the importance of the altered inductance tuning is significant when the structure is excited by a load which excites other vibration modes, while the structural damping alone only has minor influence on the series inductance tuning. Furthermore, the explicit frequency response is shown to be in very good agreement with the exact response obtained by evaluation of the vibration problem for the full flexible structure.

Finally, the explicit charge and voltage frequency response for, respectively SC and OC piezoelectric electrodes, have been used to derive an equivalent dynamic capacitance around the target resonance frequency. This dynamic capacitance is found to recover the modal capacitance commonly used for piezoelectric LR-shunt tuning at a frequency between the SC and OC frequencies, while it may also be evaluated precisely by the peak values of the frequency response for SC charge and OC voltage multiplied by the SC to OC frequency ratio.

Funding

This research has been supported by the Danish Council for Independent Research via the project 'Resonant Piezoelectric Shunt Damping of Structures'.

Appendix A.

The resulting displacements of a moderately damped structure with an LR-shunted piezoelectric material and excited by an arbitrary load is obtained by inserting the modal coefficients (31) and (32) and static deflection (23) in the modal representation (22), which yields the FRF

$$\begin{aligned}\mathbf{u} = \sum_{j=1}^{r-1} \mathbf{u}_j \frac{f_j}{X_j(\omega)} + \mathbf{u}_r \frac{Y_r(\omega)}{P_r(\omega)} f_r + \hat{\mathbf{u}}_r \frac{1}{P_r(\omega)} \hat{f}_r + \mathbf{u}_s + \left(\hat{\mathbf{u}}_r - \mathbf{u}_r - \sum_{j=1}^{r-1} \mathbf{u}_j \frac{Q_j \hat{V}_r}{X_j(\omega)} \right) \\ \times \left[\left(\frac{X_r(\omega) Y_r(\omega)}{P_r(\omega)} + \frac{C_p'(\omega)}{\Delta C_r(\omega)} \right) \frac{f_r - \hat{f}_r}{Q_r \hat{V}_r} + \sum_{j=1}^{r-1} \frac{C_j}{\Delta C_r(\omega)} \frac{V_j}{V_r} \frac{f_j}{X_j(\omega)} \right]\end{aligned} \tag{A.1}$$

However, when having fairly separated resonance frequencies, whereby $1/X_j(\omega) \to 0$, the terms containing this factor in (A.1) may be omitted, whereby the resulting displacements can be written as in (33).

Appendix B.

The present appendix presents the full expression for the voltage derivatives and squared characteristic polynomial, derived in section 5.2.

Inserting the admittance function (35) and the frequency function (15) into the voltage derivative (34), the full solution at $\omega = \omega_r$ for the parallel shunt, can be written as

$$\begin{aligned}\frac{V'(\omega_r) Q_r}{f_r} = \frac{2\omega_r Q_r \hat{V}_r}{P_r^2(\omega)} \left[\frac{\hat{f}_r}{f_r} - \lambda_r + \frac{4\zeta_r^2}{\kappa_r^2} \left(1 - \frac{\hat{f}_r}{f_r} \right) \lambda_r \right. \\ \left. - \mathrm{i} \left(\zeta_r \left(\frac{\hat{f}_r}{f_r} + \lambda_r \right) + \rho_r - \frac{2\zeta_r^2}{\kappa_r^2} \left(1 - \frac{\hat{f}_r}{f_r} \right) \rho_r \right) \right]\end{aligned} \tag{B.1}$$

which reduces to (37) when assuming moderate structural damping.

The full expression for the square of the characteristic polynomial (38) is given by

$$\left(\frac{P_r(\omega_r)}{Q_r \hat{V}_r} \right)^2 = \left(1 + \frac{2\zeta_r}{\kappa_r^2} \rho_r \right)^2 - \frac{4\zeta_r^2}{\kappa_r^4} (1 - \lambda_r)^2 + \frac{4\mathrm{i}\zeta_r}{\kappa_r^2} \left(1 + \frac{2\zeta_r}{\kappa_r^2} \rho_r \right) (1 - \lambda_r) \tag{B.2}$$

which reduces to (39) when the inductance is tuned to the SC frequency ω_r.

The real and imaginary parts of the voltage derivative (37) are separated by multiplying and dividing with the complex conjugate of the squared characteristic polynomial (39), giving the voltage derivative

$$\frac{V'(\omega_r)Q_r}{f_r} \simeq Q_r\hat{V}_r\frac{2\omega_r\bar{P}_r^2(\omega)}{P_r^2(\omega)\bar{P}_r^2(\omega)}\left[\frac{\hat{f}_r}{f_r}-\lambda_r-\mathrm{i}\left(\zeta_r\left(\frac{\hat{f}_r}{f_r}+\lambda_r\right)+\rho_r\right)\right] \tag{B.3}$$

Appendix C.

The present appendix presents the full expression for the square of the altered characteristic polynomial (43) in section 5.2, which is given by

$$\left(\frac{\hat{P}_r(\hat{\omega}_r)}{Q_r\hat{V}_r}\right)^2=\left(1+\frac{2\zeta_r}{\kappa_r^2}\frac{\hat{\omega}_r}{\omega_r}\hat{\rho}_r\right)^2-\frac{4\zeta_r^2}{\kappa_r^4}\frac{\hat{\omega}_r^2}{\omega_r^2}(1-\hat{\lambda}_r)^2-\frac{4\mathrm{i}\zeta_r}{\kappa_r^2}\frac{\hat{\omega}_r}{\omega_r}\left(1+\frac{2\zeta_r}{\kappa_r^2}\frac{\hat{\omega}_r}{\omega_r}\hat{\rho}_r\right)(1-\hat{\lambda}_r) \tag{C.1}$$

This expression reduces to (49) when the inductance is tuned to the OC frequency $\hat{\omega}_r$.

Appendix D.

The equivalent dynamic capacitance (53) evaluated at the intermediate frequency (56) is given by (57), which may be written as

$$|\bar{C}(\tilde{\omega}_r)|=C_r\left|1-\frac{2}{1+4\mathrm{i}\zeta_r\frac{\omega_r\tilde{\omega}_r}{Q_r\hat{V}_r}}\right| \tag{D.1}$$

in which the complex term in the denominator of the fraction may be eliminated by multiplying and dividing with the conjugate of the denominator, which gives

$$|\bar{C}(\tilde{\omega}_r)|=C_r\left|\frac{\left(4\zeta_r\frac{\omega_r\tilde{\omega}_r}{Q_r\hat{V}_r}\right)^2-1+2\mathrm{i}\left(4\zeta_r\frac{\omega_r\tilde{\omega}_r}{Q_r\hat{V}_r}\right)}{1+\left(4\zeta_r\frac{\omega_r\tilde{\omega}_r}{Q_r\hat{V}_r}\right)^2}\right| \tag{D.2}$$

Finally, the absolute value can be evaluated as

$$|\bar{C}(\tilde{\omega}_r)|=C_r\sqrt{\frac{1+\left(4\zeta_r\frac{\omega_r\tilde{\omega}_r}{Q_r\hat{V}_r}\right)^4-2\left(4\zeta_r\frac{\omega_r\tilde{\omega}_r}{Q_r\hat{V}_r}\right)^2+4\left(4\zeta_r\frac{\omega_r\tilde{\omega}_r}{Q_r\hat{V}_r}\right)^2}{1+\left(4\zeta_r\frac{\omega_r\tilde{\omega}_r}{Q_r\hat{V}_r}\right)^4+2\left(4\zeta_r\frac{\omega_r\tilde{\omega}_r}{Q_r\hat{V}_r}\right)^2}}=C_r \tag{D.3}$$

whereby it is seen that the square root becomes unity so that the equivalent dynamic capacitance equals the modal capacitance C_r at the intermediate frequency $\tilde{\omega}_r$.

The modal capacitance C_r may be determined from the charge $\bar{Q}(\omega)$ and OC Voltage $\bar{V}(\hat{\omega}_r)$ measured at the SC and OC frequencies, respectively. The relation between these peak values is given by

$$\bar{C}_r=-\frac{\bar{Q}(\omega_r)}{\bar{V}(\hat{\omega}_r)}=C_r\left|\frac{\hat{\omega}_r-2\mathrm{i}\zeta_r\frac{\hat{\omega}_r}{\kappa_r^2}\left(1-\frac{\hat{f}_r}{f_r}\right)}{\omega_r\frac{\hat{f}_r}{f_r}-2\mathrm{i}\zeta_r\frac{\hat{\omega}_r}{\kappa_r^2}\left(1-\frac{\hat{f}_r}{f_r}\right)}\right| \tag{D.4}$$

when using the FRFs for the SC charge and OC voltage in (52). By multiplying with the conjugate of the denominator, the real and imaginary parts of (D.4) can be separated as

$$\bar{C}_r = C_r \left| \frac{\omega_r \hat{\omega}_r \frac{\hat{f}_r}{f_r} + 4\zeta_r^2 \frac{\hat{\omega}_r^2}{\kappa_r^4} \left(1 - \frac{\hat{f}_r}{f_r}\right)^2 - 2\mathrm{i}\zeta_r \frac{\hat{\omega}_r}{\omega_r} \frac{\omega_r^2}{\kappa_r^2} \left(1 - \frac{\hat{f}_r}{f_r}\right) \left(\frac{\hat{\omega}_r}{\omega_r} - \frac{\hat{f}_r}{f_r}\right)}{\omega_r^2 \left(\frac{\hat{f}_r}{f_r}\right)^2 + 4\zeta_r^2 \frac{\hat{\omega}_r^2}{\kappa_r^4} \left(1 - \frac{\hat{f}_r}{f_r}\right)^2} \right| \tag{D.5}$$

It is here seen that both the second term in the numerator and denominator tends to zero as both ζ_r^2 and $(1 - \hat{f}_r/f_r)^2$ vanish. Expression (D.5) may therefore be written as

$$\bar{C}_r \simeq C_r \frac{\hat{\omega}_r}{\omega_r} \frac{f_r}{\hat{f}_r} \left| 1 - 2\mathrm{i} \frac{\zeta_r}{\kappa_r^2} \frac{f_r}{\hat{f}_r} \left(1 - \frac{\hat{f}_r}{f_r}\right) \left(\frac{\hat{\omega}_r}{\omega_r} - \frac{\hat{f}_r}{f_r}\right) \right| \tag{D.6}$$

Finally, upon evaluation of the absolute value, (D.6) is given by

$$\bar{C}_r \simeq C_r \frac{\hat{\omega}_r}{\omega_r} \frac{f_r}{\hat{f}_r} \sqrt{1 + 4\frac{\zeta_r^2}{\kappa_r^4} \left(\frac{f_r}{\hat{f}_r}\right)^2 \left(1 - \frac{\hat{f}_r}{f_r}\right)^2 \left(\frac{\hat{\omega}_r}{\omega_r} - \frac{\hat{f}_r}{f_r}\right)^2} \tag{D.7}$$

Again it is seen that the term containing the factors ζ_r^2 and $(1 - \hat{f}_r/f_r)(\hat{\omega}_r/\omega_r - \hat{f}_r/f_r)$ vanishes for moderate structural damping, whereby the relation between the measured peak charge and voltage is accurately related to the modal capacitance by the expression in (58).

References

[1] S. Behrens, A.J. Fleming, S.O.R. Moheimani, A broadband controller for shunt piezoelectric damping of structural vibration, Smart Mater. Struct. 12 (2003) 18-28.

[2] B. de Marneffe and A. Preumont, Vibration damping with negative capacitance shunts: theory and experiment, Smart Mater. Struct. 17 (2008) 035015. https://doi:10.1088/0964-1726/17/3/035015.

[3] M. Berardengo, O. Thomas, C. Giraud-Audine, S. Manzoni, Improved resistive shunt by means of negative capacitance: new circuit, performances and multi-mode control, Smart Mater. Struct. 25 (2016) 075033. https://doi:10.1088/0964-1726/25/7/075033.

[4] M. Berardengo, S. Manzoni,O. Thomas, M. Vanali, Piezoelectric resonant shunt enhancement by negative capacitances: Optimisation, performance and resonance cancellation, J. Intell. Mater. Syst. Struct. 29(12) (2018) 2581-2606. https://doi.org/10.1177/1045389X18770874.

[5] J. Ducarne, O. Thomas, J.-F. Deü, Structural Vibration Reduction by Switch Shunting of Piezoelectric Elements: Modeling and Optimization, J. Intell. Mater. Syst. Struct. 21 (2010) 797-816. https://doi:10.1177/1045389X10367835.

[6] E.H. Anderson, N.W. Hagood, Simultaneous piezoelectric sensing/actuation: Analysis and application to controlled structures, J. Sound Vib. 174 (1994) 617-639. https://doi.org/10.1006/jsvi.1994.1298.

[7] A. Preumont, Vibration Control of Active Structures, An Introduction. 3rd edition Springer Heidelberg, 2011.

[8] M. Lallart, E. Lefeuvre, C. Richard, D. Guyomar, Self-powered circuit for broadband, multimodal piezoelectric vibration control, Sens. Actuators A: Phys. 143, (2008) 377-382. https://doi.org/10.1016/j.sna.2007.11.017.

[9] A.J. Fleming, S. Behrens, S.O.R. Moheimani, Synthetic impedance for implementation of piezoelectric shunt-damping circuits, Electronics Letters 36 (2000) 1525-1526. http://dx.doi.org/10.1049/el:20001083.

[10] O. Thomas, J. Ducarne, J.-F. Deü, Performance of piezoelectric shunts for vibration reduction, Smart Mater. Struct. 21(1) (2012) 015008. https://doi:10.1088/0964-1726/21/1/015008.

[11] B. Lossouarn, M. Aucejo, J.-F. Deü, B. Multon, Design of inductors with high inductance values for resonant piezoelectric damping, Sens. Actuators A: Phys. 259 (2017) 68-76. https://doi.org/10.1016/j.sna.2017.03.030.

[12] B. Lossouarn, J.-F. Deü, G. Kerschen, A fully passive nonlinear piezoelectric vibration absorber, Phil.Trans.R. Soc. A 376 (2018) 20170142. https://doi.org/10.1098/rsta.2017.0142.

[13] J.F. Toftekær, J. Høgsberg, Experimental Validation of Piezoelectric Shunt Tuning with Residual Mode Correction: Damping of Plate-Like Structures, J. Intell. Mater. Syst. Struct. 31(9) (2020) 1220-1239. https://doi.org/10.1177/1045389X20914393.

[14] G. Matten, M. Collet, S. Cogana, E. Sadoulet-Reboula, Synthetic impedance for adaptive piezoelectric metacomposite, Procedia Technology 15 (2014) 84-89.

[15] G. Raze, A. Jadoul, S. Guichaux, V. Broun, G. Kerschen, A digital nonlinear piezoelectric tuned vibration absorber, Smart Mater. Struct. 29 (2019) 015007. https://doi.org/10.1088/1361-665X/ab5176.

[16] R.L. Forward, Electronic damping of vibrations in optical structures, Appl. Optics. 18, (1979) 690-697. https://doi.org/10.1364/AO.18.000690.

[17] N.W. Hagood, A. von Flotow, Damping of structural vibrations with piezoelectric materials and passive electrical networks, J. Sound Vib. 146 (1991) 243-268. https://doi.org/10.1016/0022-460X(91)90762-9.

[18] S.Y. Wu, Piezoelectric shunts with a parallel R-L circuit for structural damping and vibration control, In Proc. SPIE 2720 (1996) 259-269. https://doi.org/10.1117/12.239093.

[19] J.J. Hollkamp, Multimodal passive vibration suppression with piezoelectric materials and resonant shunts, *J. Intell. Mater. Syst. Struct.* 5(1994) 49-57. https://doi.org/10.1177/1045389X9400500106.

[20] J. Høgsberg, S. Krenk, Balanced calibration of resonant shunt circuits for piezoelectric vibration control, J. Intell. Mater. Syst. Struct. 23 (2012) 1937-1948. https://doi.org/10.1177/1045389X12455727.

[21] P. Soltani, G. Kerschen, G. Tondreau, A. Deraemaeker, Piezoelectric vibration damping using resonant shunt circuits: an exact solution, Smart Mater. Struct. 23 (2014) 125014, https://doi:10.1088/0964-1726/23/12/125014.

[22] P. Soltani, G. Kerschen, G. Tondreau, A. Deraemaeker, Tuning of a piezoelectric vibration absorber attached to a damped structure, J. Intell. Mater. Syst. Struct. 28 (2016) 1115-1129. https://doi:10.1177/1045389X16666180.

[23] C. Park, D. Inman, Uniform model for series R-L and parallel R-L shunt circuits and power consumption, Proc. SPIE 3668, Smart Struct. Mater. (1999) 797-804. https://doi.org/10.1117/12.350755.

[24] G. Caruso, A critical analysis of electric shunt circuits employed in piezoelectric passive vibration damping, Smart Mater Struct. 10 (2001) 1059-1068.

[25] P. Gardonio, D. Casagrande, Shunted piezoelectric patch vibration absorber on two-dimensional thin structure: tuning considerations, J. Sound Vib. 395 (2017) 26-47. https://doi.org/10.1016/j.jsv.2017.02.019.

[26] W. Larbi, J.-F. Deü, Reduced order finite element formulations for vibration reduction using piezoelectric shunt damping, Appl. Acoust. 147 (2019) 111-120. htps://doi.org/10.1016/j.apacoust.2018.04.016.

[27] J. Høgsberg, S. Krenk, Calibration of piezoelectric RL shunts with explicit residual mode correction, J. Sound Vib. 386 (2017) 65-81. https://doi.org/10.1016/j.jsv.2016.08.028.

[28] J.F. Toftekær, A. Benjeddou, J. Høgsberg, S. Krenk, Optimal piezoelectric RL shunt damping of plates with residual mode correction, J. Intell. Mater. Syst. Struct. 29 (2018) 3346-3370. https://doi.org/10.1177/1045389X18798953.

[29] J.F. Toftekær, J. Høgsberg, Multi-Mode Piezoelectric Shunt Damping with Residual Mode Correction by Evaluation of Modal Charge and Voltage, J. Intell. Mater. Syst. Struct. 31(4) (2020) 570-586. https://doi.org/10.1177/1045389X19891646.

[30] J.A. Main, S. Krenk, Efficiency and tuning of viscous dampers on discrete systems, J. Sound Vib. 286 (2005) 97-122. http://dx.doi.org/10.1016/j.jsv.2004.09.022.

[31] IEEE Inc., Standards on piezoelectricity, ANS/IEEE Std 176-1987 USA, 1988.

[32] Porfiri M, Maurini C and Pouget J Identification of electromechanical modal parameters of linear piezoelectric structures, Smart Mater. Struct. 16 (2007) 323-331.

[33] J. Høgsberg, Consistent frequency-matching calibration procedure for electromechanical shunt absorbers, J. Vib. Control. 26 (2020) 1133-1144. https://doi.org/10.1177/1077546320924207.

[34] R. Darleux, B. Lossouarn, J.-F. Deü, Passive self-tuning inductor for piezoelectric shunt damping considering temperature variations, J. Sound Vib. 432 (2018) 105-118. https://doi.org/10.1016/j.jsv.2018.06.017.

[35] A. Benjeddou, Advances in piezoelectric finite element modeling of adaptive structural elements: a survey, Comput. Struct. 76 (2000) 347-363.

[36] J.F. Toftekær, A. Benjeddou, J. Høgsberg, General numerical implementation of a new piezoelectric shunt tuning method based on the effective electromechanical coupling coefficient, *Mech. Adv. Mater. Struc.* 27:22 (2020) 1908-1922. https://doi.org/10.1080/15376494.2018.1549297.

[37] S. Krenk, Frequency analysis of the tuned mass damper, J. Appl. Mech. 72 (2005) 936-942. https://doi.org/10.1115/1.2062867.